

# Utilization of a Fifth-Order Model for Analyzing Stirling Oscillators

Shahriar Niknejad<sup>a</sup> | Amir Fassih<sup>a</sup> | Amir Mobini<sup>a</sup> Heybatollah Jokar<sup>b</sup> | Shahryar Zare<sup>a,\*</sup>

a Department of Mechanical Engineering, Iranian Research Organization for Science and Technology (IROST)
 b Department of Mechanical Engineering, Firouzabad Higher Education Center, Shiraz University of Technology, Shiraz, Iran
 \* Corresponding author, Email: sh.zare@irost.ir

#### **Article Information**

#### Article Type

RESEARCH ARTICLE

#### **Article History**

RECEIVED: 30 Jun 2025 REVISED: 13 Sep 2025 ACCEPTED: 01 Oct 2025

Published Online: 05 Oct 2025

#### Keywords

Free piston Stirling oscillators Fifth-order model Renewable energy Dynamic analysis

#### Abstract

In this study, for the first time, the design of a free-piston Stirling oscillator (FPSO) using a fifth-order model is addressed. Initially, the free-piston Stirling oscillator is introduced. Then, considering the limited heat transfer coefficient, the fifth-order mechanical model of the oscillator is derived. Subsequently, the design parameters, including the stiffness and mass of the power piston and displacer piston, as well as the cross-sectional area of the rod connecting to the displacer piston, are examined. Then, the design parameters are estimated based on the objectives (a desired frequency between 70 and 100 rad/s, and the real value of the dominant closed-loop pole between 5 and 17) and the fifth-order mechanical model. Nonlinear analysis is then performed to investigate the effects of variations in frequency and the real value of the dominant closed-loop poles on the output power and phase difference between the pistons of the oscillator. The results of this study demonstrate that the use of a fifth-order model offers a more accurate evaluation and analysis of the dynamic behavior of this type of oscillator.

Cite this article: Niknejad, S., Fassih, A., Mobini, A., Jokar, H., Zare, S. (2025). Utilization of a Fifth-Order Model for Analyzing Stirling Oscillators. DOI: 10.22104/hfe.2024.7207.1329



© The Author(s). Publisher: Iranian Research Organization for Science and Technology (IROST) DOI: 10.22104/hfe.2024.7207.1329

#### 1 Introduction

Reducing the use of fossil fuels has become one of the most significant challenges for researchers [1,2]. In response, considerable efforts have been made to harness energy from renewable sources. One innovative approach involves the use of converters known as thermal oscillators. Among these, the utilization of solar thermal energy for electricity generation is currently a major area of research [3, 4]. Various technologies, such as solar thermals, have been introduced to convert solar heat into electrical energy [5, 6]. Among the newest of these technologies are free-piston Stirling oscillators, which are capable of performing this task [7,8]. These oscillators operate based on the Stirling thermodynamic cycle [9, 10]. Free-piston Stirling oscillators offer several advantages, such as reduced mechanical friction, high frequency, and minimal maintenance requirements, due to the elimination of mechanical links [11,12]. However, these benefits also introduce challenges, particularly in the dynamics of the start-up process. As a result, extensive research has been conducted to explore the start-up behavior of this type of oscillator [13, 14].

Most research on Stirling oscillators has used a fourth-order linear model [15, 16]. In these analyses, it is assumed that the heat transfer coefficients between the heat sources and the hot and cold gas chambers are infinite, simplifying the analysis. In this context, Riofrio et al. [13] examined the linear dynamics of a free-piston Stirling oscillator (FPSO) using a fourthorder model. Their analysis indicated that increasing the temperature of the hot source leads to an increase in the real part of the dominant poles of the oscillator's dynamics, resulting in greater instability. In this study, the dynamic instability of the oscillator was also examined using Nyquist plots. Hofacker et al. [14] investigated the closed-loop poles of the oscillator using a fourth-order linear model, where the linear dynamics of the engine were analyzed based on four types of parameters. Zare and Tavakolpour-Saleh [15] designed the parameters of a Stirling oscillator based on a desired frequency, employing a fourth-order linear model. In this study, the engine's linear dynamics were analyzed at a marginally stable state. Der Minassians and Sanders [16] analyzed the dynamics of a three-phase Stirling oscillator using a fourth-order linear model. First, they derived the governing linear dynamic equations of the oscillator, then obtained the closed-loop poles. Zare and Tavakolpour-Saleh [17] designed and analyzed the dynamics of a Stirling oscillator using a fourth-order linear model combined with the Particle Swarm Optimization (PSO) method. In their study,

design parameters such as piston mass and spring stiffness were estimated using the PSO technique. Begot et al. [18] investigated the stability or instability of a Stirling oscillator's dynamics using a fourth-order mechanical model, examining the impact of the generator's additional load on the oscillator's dynamic stability or instability. Their study also assessed the selfstarting capability of the oscillator. Recently, one useful method for analyzing and evaluating the performance of Stirling oscillators is the application of artificial intelligence [19]. Artificial intelligence encompasses a range of techniques that enable computers to perform intelligent, human-like actions in decision-making across various domains [20, 21]. In other words, AI allows machines to interpret data, learn from it, and apply the acquired knowledge to perform tasks typically requiring human intelligence [22,23]. Within this framework, deep learning and machine learning techniques can be employed to train intelligent systems for a wide range of activities [24].

Most studies have relied on a fourth-order mechanical model, often overlooking the limitations of the heat transfer coefficient. However, since the startup behavior of these oscillators is directly influenced by the gas temperature in both the hot and cold spaces, more accurate estimation of these temperatures could significantly help designers in predicting the performance of this type of oscillator. Additionally, accurately knowing the temperature values in the hot and cold spaces allows for a more precise design of the system's parameters. In this paper, for the first time, the design and performance evaluation of Stirling oscillators are conducted using a fifth-order mechanical model. This approach allows the fifth-order model to account for the effects of limited heat transfer coefficients in the analysis and evaluation of Stirling oscillators. Based on the research conducted so far, no study has examined or estimated the design parameters of Stirling oscillators using a fifth-order model. Therefore, this study begins with a review and introduction to the free-piston Stirling oscillator. Next, the dynamic equations of the oscillator are derived based on a fifth-order model. The performance of the oscillator is then evaluated using this model and nonlinear equations. Subsequently, the design parameters, including the mass and stiffness of the pistons, as well as the cross-sectional area of the rod, are estimated, taking into account the desired frequency and the real part of the dominant closed-loop poles. Finally, the results of the study are analyzed.

# 2 Free Piston Stirling Oscillator

Stirling oscillators generally consist of two pistons (the displacer and power pistons), two springs (connected to

the pistons), a cylinder, and two hot and cold spaces (Figure 1) [25, 26]. As shown in Figure 1, stable oscillations in the oscillator's dynamics occur when the phase difference between the displacer and power pistons reaches a certain threshold. To achieve the desired phase difference, certain engine parameters, such as the mass of the pistons and the stiffness of their springs, must have specific values [27,28]. Another crucial parameter that can destabilize the dynamics of this type of oscillator is the temperature of the cold and hot sources, which must also be maintained within a certain range.

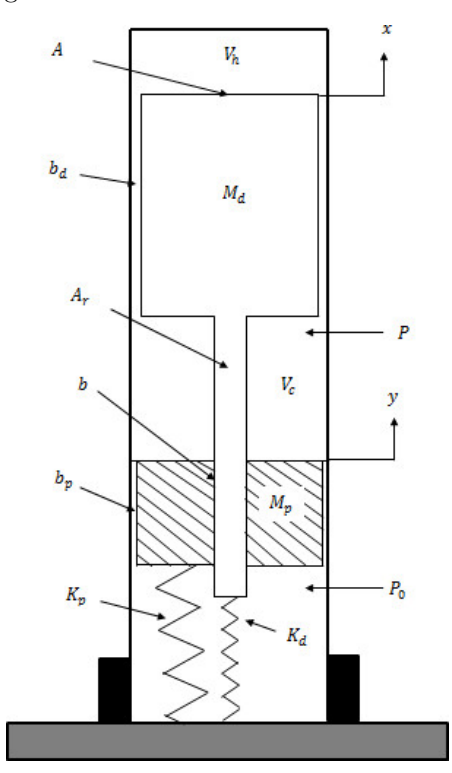


Fig. 1. Schematic view of a FPSO.

# 3 Mathematical Background

This section aims to derive both linear and nonlinear equations to investigate the impact of the real and imaginary components of the dominant poles on the engine's performance within the fifth-order model. Based on Figure 1, the governing nonlinear dynamic equations of the Stirling oscillator are as follows [29]:

$$M_p \ddot{y} + b(\dot{y} - \dot{x}) + b_p \dot{y} + K_p y + \alpha y^3$$
  
= -(P - P\_0)(A - A\_r), (1)

$$M_d \ddot{x} + b(\dot{x} - \dot{y}) + b_d \dot{x} + K_d x + \beta x^3$$
  
= -(P - P\_0) A<sub>r</sub>. (2)

By neglecting the nonlinear terms related to the stiffness of the springs connected to the pistons, the governing linear dynamic equations of the FPSO can be expressed as follows:

$$M_p \ddot{y} + b(\dot{y} - \dot{x}) + b_p \dot{y} + K_p y$$
  
= -(P - P\_0)(A - A\_r), (3)

$$M_d \ddot{x} + b(\dot{x} - \dot{y}) + b_d \dot{x} + K_d x$$
  
=  $-(P - P_0)A_r$ . (4)

Equations (3) and (4) have been derived under the assumption that heat transfer between the cold and hot sources, as well as between the cold and hot chambers, is infinite. However, in reality, heat transfer is limited, and this factor must be incorporated into the equations. To account for this, a new state variable needs to be introduced into the dynamics of the oscillator. In this context, the change in pressure is considered as the new state variable. The change in internal energy can be expressed using the energy control volume approach as follows [30]:

$$\dot{U} = \dot{H} + \dot{Q}_{\text{net}} - \dot{W} \,. \tag{5}$$

In Equation (5),  $\dot{H}$  represents the rate of change of enthalpy, which is assumed to be zero in this study. Accordingly, the rate of instantaneous pressure change can be calculated as follows:

$$\dot{U} = \frac{\dot{P}V + P\dot{V}}{\gamma - 1} = \dot{Q}_{\text{net}} - \dot{P}V, \qquad (6)$$

$$\dot{P} = \frac{(\gamma - 1)(\dot{Q}_{\rm in} + \dot{Q}_{\rm out} + \dot{Q}_{\rm wall}) - \gamma P \dot{V}}{V}, \quad (7)$$

where:

$$\dot{Q}_{\rm in} = h_h A_h (T_h - T) \,, \tag{8}$$

$$\dot{Q}_{\text{out}} = h_c A_c (T_c - T) \,, \tag{9}$$

$$\dot{Q}_{\text{wall}} = h_{\text{wall}} A_{\text{wall}} (T_{\text{wall}} - T), \qquad (10)$$

$$A_h = x\pi d + A_{h0} \,, \tag{11}$$

$$A_c = (x - y)\pi d + A_{c0}. (12)$$

The changes in volume in the cold and hot spaces are given by the following expressions:

$$V_h = V_{h0} - Ax, (13)$$

$$V_c = V_{c0} - (A - A_r)(y - x). (14)$$

With these explanations, the time derivative of the changes in the cold, hot, and total volume of the cylinder is expressed as follows:

$$\dot{V}_h = -A\dot{x}\,, (15)$$

$$\dot{V}_c = -(A - A_r)(\dot{y} - \dot{x}),$$
 (16)

$$V = V_c + V_h = V_{h0} + V_{c0} - (A - A_r)y - A_r x, \quad (17)$$

$$\dot{V} = -(A - A_r)\dot{y} - A_r\dot{x}. \tag{18}$$

By substituting Equations (8) to (18) into Equation (7), the rate of change of pressure is obtained as follows:

$$\dot{P} = \frac{(\gamma - 1)[h_h A_h (T_h - T) + h_c A_c (T_c - T) + h_{\text{wall}} A_{\text{wall}} (T_{\text{wall}} - T)] + \gamma P[(A - A_r)\dot{y} + A_r \dot{x}]}{V_{h0} + V_{c0} - (A - A_r)y - A_r x}$$
(19)

To analyze the linear dynamics of the oscillator, it is necessary to linearize the relationship concerning the rate of change of pressure:

$$\dot{P} = c_1(y - y_0) + c_2(x - x_0) + c_3(\dot{y} - \dot{y}_0) + c_4(\dot{x} - \dot{x}_0) + c_5(P - P_0) \quad (20)$$

The values of  $c_1$  to  $c_5$  can be found in [14].

Based on the explanations provided, the state variables for the system (accounting for limited heat transfer) are defined as follows:

$$x_1 = y \tag{21}$$

$$x_2 = \dot{y} \tag{22}$$

$$x_3 = x \tag{23}$$

$$x_4 = \dot{x} \tag{24}$$

$$x_5 = P - P_0 (25)$$

Based on Equations (20) to (25), along with the governing dynamic equations of the oscillator (i.e., Equations (3) and (4)), the closed-loop matrix is obtained as follows:

$$\begin{bmatrix} \dot{x} \\ \ddot{x} \\ \dot{y} \\ \ddot{y} \\ \dot{P} \end{bmatrix} = \begin{bmatrix} 0 & 1 & 0 & 0 & 0 \\ -\frac{K_d}{M_d} & -\frac{b_d+b}{M_d} & 0 & \frac{b}{M_d} & \frac{A_r}{M_d} \\ 0 & 0 & 0 & 1 & 0 \\ 0 & \frac{b}{M_p} & -\frac{K_p}{M_p} & -\frac{b_p+b}{M_p} & \frac{A-A_r}{M_p} \\ c_1 & c_2 & c_3 & c_4 & c_5 \end{bmatrix} \begin{bmatrix} x \\ \dot{x} \\ y \\ \dot{y} \\ P \end{bmatrix}$$

$$(26)$$

As indicated by Equation (26), the closed-loop matrix of the engine, accounting for the limited heat transfer coefficient, has five eigenvalues (poles). Consequently, this analysis will be conducted according to a fifth-order model. In other words, this paper aims to provide a more accurate dynamic analysis of FPSO by incorporating the effect of limited heat transfer. Figure 2 presents a schematic representation of the closed-loop poles of the engine in the fifth-order analysis. According to Figure 2, this analysis reveals two dominant poles and three non-dominant poles, with the behavior of the system being primarily determined by the dominant poles.

#### 4 Results and Discussion

The goal of this section is to examine and evaluate the fifth-order model. Accordingly, the model's performance and efficiency will be assessed by comparing its results with nonlinear analysis. Subsequently, the design parameters will be estimated based on two specified objectives: the desired frequency and the real part of the dominant poles.

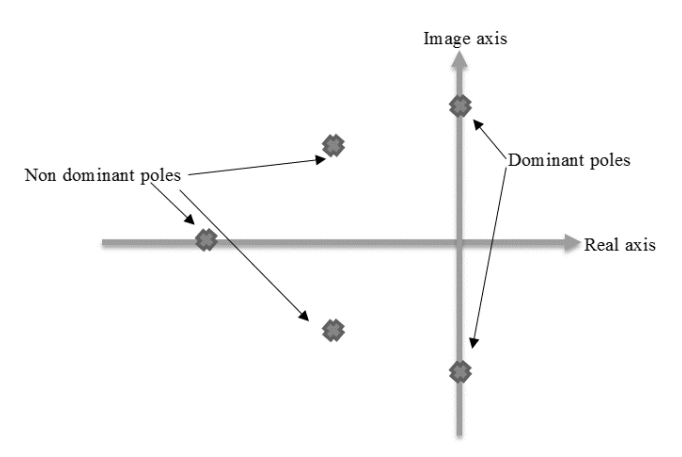


Fig. 2. Schematic view of the locations of the closed-loop poles (5<sup>th</sup> order model).

#### 4.1 Evaluation of the fifth-order model

In the previous section, the nonlinear and linear governing equations of the oscillator were derived. As shown in Equation (26), in the analysis using the fifth-order model, the system dynamics in the linear state have five closed-loop poles, two of which are dominant and determine the oscillator's dynamic behavior. In linear analysis, the imaginary and real parts of the dominant closed-loop poles correspond to the oscillator's frequency and output power, respectively. In this study, data from the B10-B free-piston Stirling oscillator model is used to assess the performance of the fifth-order model. The specifications of this oscillator are provided in Table 1.

Table 1. B10-B Specifications [30].

Parameter	Value	Parameter	Value
$\overline{A}$	$0.00101\mathrm{m}^2$	$M_d$	$0.086\mathrm{kg}$
$P_0$	100  kpa	$M_p$	0.529  kg
M	$4.58 \times 10^{-5} \text{ kg}$	$K_d$	$600  \mathrm{Nm}^{-1}$
$K_p$	$650  {\rm Nm^{-1}}$		

Based on Table 1 and the closed-loop system matrix (Equation (26)), the values of the oscillator's closed-loop poles are calculated in Table 2.

Table 2. Closed-loop poles based on the fifth-order model.

Poles	Dominant poles	Non-dominant poles
B10-B	9.18 + 83.11j, $9.18 + 83.11j$	-37.26 + 81.16j, -37.26 + 81.16j, -43.66

Based on the dominant poles of the system, the main frequency of the B10-B is calculated to be 83.11 rad/s. To assess the performance of the presented linear analysis, the oscillator's dynamic behavior is also evaluated using nonlinear equations (Equations (1) and (2)). Given the specifications of the B10-B, provided in Table 2, the variations in the velocities of the displacer and power pistons have been simulated, as shown in Figure 3. Additionally, Figure 4 depictes the oscillations of the displacer and power pistons. Based on Figures 3 and 4, and the number of cycles occurring within a one-second interval, the frequency of the oscillator in the nonlinear state is found to be 81.1 rad/s.

Comparing the frequency calculated by the fifth-order linear method (the imaginary part of the dominant closed-loop pole) with the frequency obtained from nonlinear analysis shows that the results of the presented linear method are valid and can be used to analyze the oscillator's performance. It is worth mentioning that the oscillator's experimentally measured frequency is 80.1 rad/s. It is worth mentioning that the operating frequency of the oscillator is determined to be 84.34 Hz using the fourth-order method. When comparing the operating frequencies obtained using the fourth-order method (84.34 Hz), the fifth-order method (80.3 Hz), it is evident that the fifth-order method provides a more accurate prediction with less error.

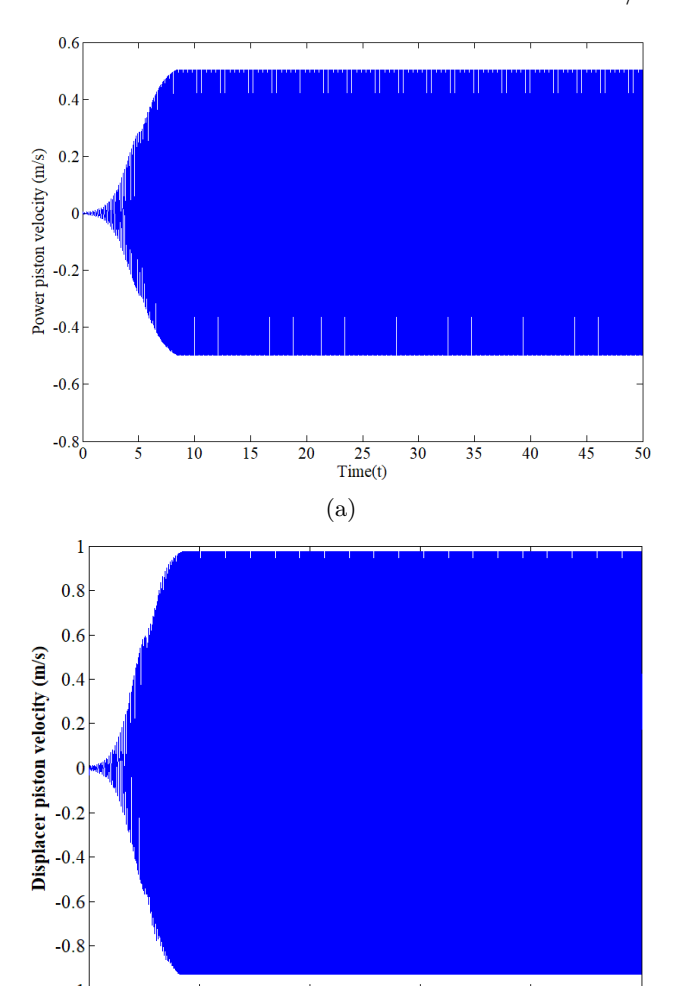


Fig. 3. Velocity of pistons (a) power piston (b) displacer piston.

**Time (t)** (b)

40

50

10

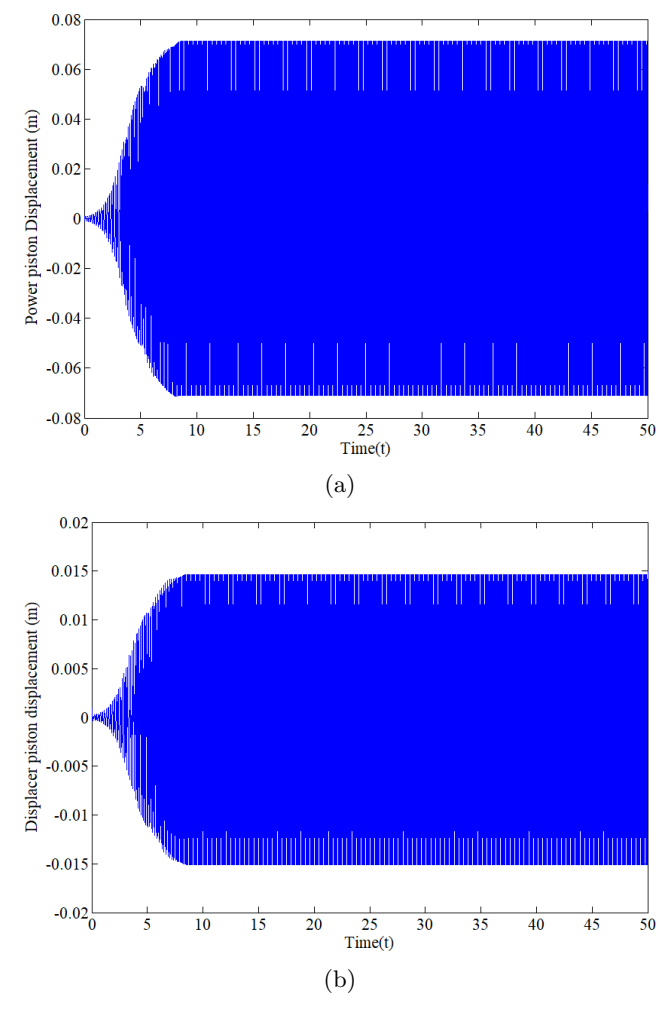


Fig. 4. Fluctuations of pistons (a) power piston (b) displacer piston.

As the results indicate, the fifth-order linear method proves to be a valid tool for analyzing the oscillator's performance. Additionally, it was shown that the imaginary part of the dominant poles corresponds to the oscillator's frequency, while the real part represents the output power. With this understanding, it becomes possible to design key oscillator parameters based on the desired frequency or the real part of the dominant closed-loop poles. This approach is further explored in subsection 4.2.

# 4.2 Designing oscillator parameters based on desired objectives

In this section, the aim is to assess the oscillator's performance based on the fifth-order linear analysis. This evaluation will be conducted using two approaches. The first approach involves designing the oscillator parameters according to the desired frequency (the imaginary value of the dominant poles). The second objective is to design the oscillator based on the desired value of the real value of the dominant poles. In this study, the mass of the pistons, the stiffness of the pistons' springs, and the cross-sectional area of the rod are considered as the key design parameters. In the first step, the desired frequency of the oscillator is chosen within a range of 70 to 100 rad/s, based on the physical characteristics of the oscillator. By solving five linear equations simultaneously (since there are four design parameters and four equations, the Newton-Raphson method is used to estimate the solutions), the corresponding design parameters can be determined. Table 3 presents the estimated values of the design parameters based on the desired operating frequencies.

Table 3. Design parameter values based on the desired frequency (The real value of the dominant closed-loop poles was fixed at 9.18)

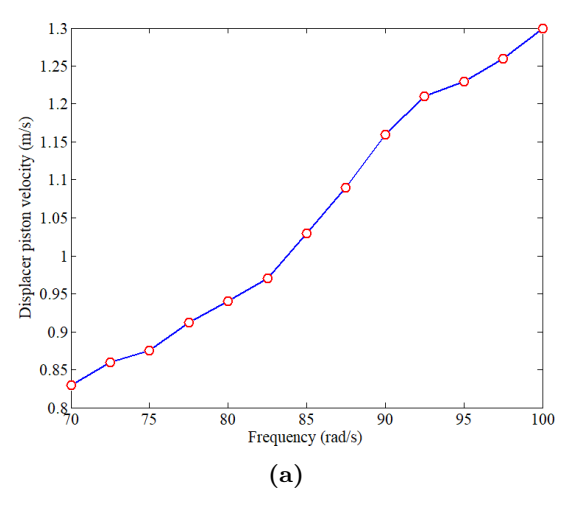
Design parameter	Imaginary Values of Dominant Poles							
Design parameter	(70)	(72.5)	(75)	(77.5)	(80)	(82.5)	(85)	(87.5)
$M_p$ (kg)	0.69	0.713	0.745	0.623	0.561	0.531	0.524	0.515
$M_d$ (kg)	0.1	0.098	0.087	0.106	0.089	0.087	0.085	0.082
$K_p  (\mathrm{Nm}^{-1})$	421	489	547	489	571	645	667	661
$K_d  (\mathrm{Nm}^{-1})$	310	427	502	533	561	604	602	611
$A_r  (\mathrm{m}^2)$	0.00013	0.00013	0.00014	0.00015	0.00015	0.00016	0.000172	0.000172
Design parameter			Imagin	nary Values	of Domina	nt Poles		
Design parameter	(90)	(92.5)	(95)	(97.5)	(100)			
$M_p$ (kg)	0.518	0.501	0.488	0.487	0.478			
$M_d$ (kg)	0.08	0.083	0.076	0.079	0.077			
$K_p  (\mathrm{Nm}^{-1})$	650	621	611	616	650			
$K_d  (\mathrm{Nm}^{-1})$	608	597	577	634	654			
$A_r (\mathrm{m}^2)$	0.00017	0.00017	0.00017	0.000171	0.00017			

# 4.3 The impact of frequency and the real value of the dominant pole on oscillator performance

As mentioned in subsection 4.1, the results from the fifth-order linear analysis align well with those obtained through nonlinear analysis. Therefore, by applying nonlinear analysis and using the estimated parameter values derived from the fifth-order model, we can effectively analyze and evaluate the oscillator's performance. In the first analysis, we will examine the impact of increasing frequency on the maximum speed and displacement of the pistons. Specifically, by selecting the desired frequency (as shown in Table 3), the values of the design parameters will change, which will lead to corresponding changes in the pistons' speed and displacement. Figure 5 illustrates the effect of varying frequency on the maximum velocity of both the dis-

placer and power pistons. As shown, an increase in frequency leads to a higher velocity of the pistons, which can be beneficial for designers. Specifically, increasing the frequency from 70 rad/s to 100 rad/s results in the power piston's velocity rising from 0.43 m/s to  $0.527\,\text{m/s}$ . Similarly, the velocity of the displacer piston increases from  $0.83\,\text{m/s}$  to  $1.3\,\text{m/s}$ .

Figure 6 also illustrates the effect of varying the frequency on the amplitude of the pistons' oscillations. As shown in Figure 6, an increase in frequency results in a rise in the pistons' displacement amplitude. It is noteworthy that increasing the amplitude of the power piston's fluctuations is highly desirable for designers aiming to produce greater power. Specifically, raising the frequency from 70 rad/s to 100 rad/s leads to an increase in the displacement amplitude of the power piston from 0.051 m to 0.0802 m.



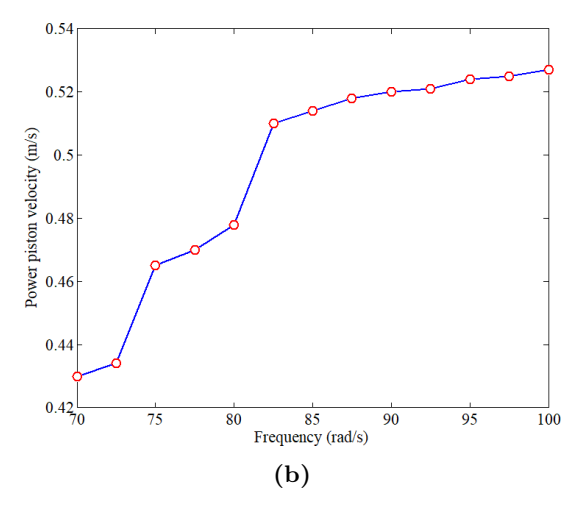
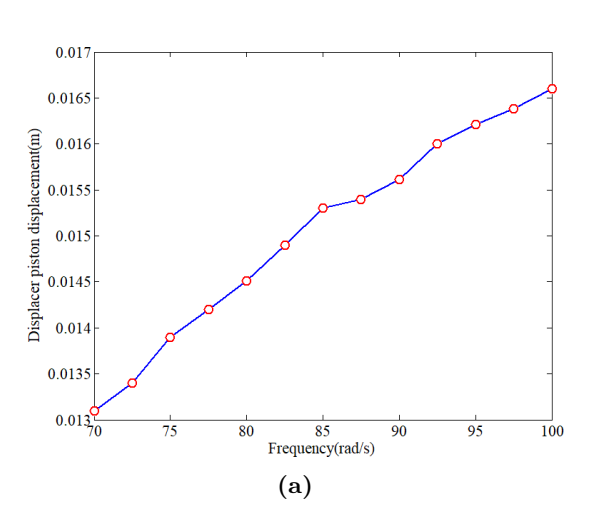


Fig. 5. The effect of changing the frequency on the maximum velocity of pistons (a) displacer piston (b) power piston.



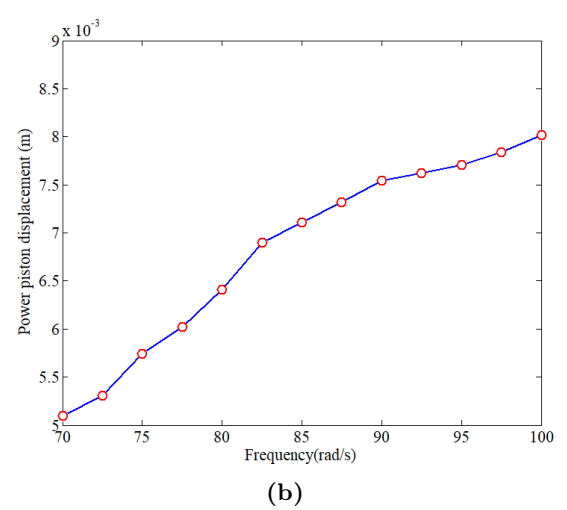


Fig. 6. The effect of changing the frequency on the maximum amplitude of pistons (a) displacer piston (b) power piston.

Figure 7 illustrates the effect of varying the real part of the closed-loop poles on the pistons' velocity. As shown, as the real value of the dominant closedloop poles increases from 5 to 17, the velocity of the power piston rises from 0.86 m/s to 1.3 m/s. Similarly, this increase also boosts the velocity of the displacer piston, from 0.463 m/s to 0.5241 m/s. In this context, an increase in the real part of the poles leads to a longer stroke length for both the power and displacer pistons, as illustrated in Figure 8. As shown, increasing the real part of the poles from 5 to 17 results in the stroke length of the power piston increasing from 0.057 meters to 0.0754 meters. Similarly, the stroke length of the displacer piston rises from 0.0136 meters to 0.0162 meters. These results indicate that as the real part of the dominant poles increases, the oscillator's performance improves, leading to greater instability and enhanced efficiency.

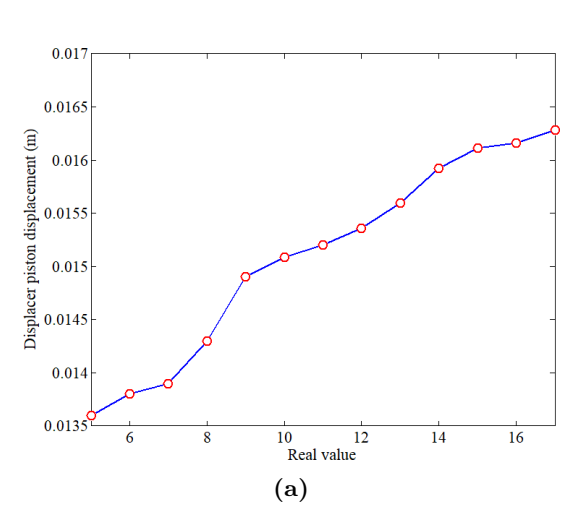
In conclusion, by simulating the P-V diagram of the oscillator for each of the parameter values calculated in Tables 3 and 4, the oscillator's performance in terms of output power can be effectively evaluated. Figures 9 and 10 demonstrate the effects of varying the real part of the poles and the operating frequency on the oscillator's output power. The results shown in these figures reveal that increases in both the real part of the poles and the operating frequency contribute to significant improvements in the oscillator's output power. The phase difference between the pistons is one of the crucial factors for the startup and optimal performance of free-piston Stirling oscillators. By simulating the behavior of the pistons based on the nonlinear governing equations of the oscillator, using the parameter values from Tables 3 and 4, the phase difference between the pistons can be calculated. As expected, increases in the frequency and the real part of the poles lead to an improvement in the phase difference between the pistons (see Figures 11 and 12). Overall, the fifth-order model successfully evaluated the performance of the FPSO,

with results that closely align with those from the non-linear model. As a result, this model can be used to analyze the initial startup of Stirling oscillators.

Table 4. Design parameter values based on the desired real value of dominant poles (Imaginary parts of the dominant closed-loop poles were fixed at 83.11 rad/s)

Design parameter (5) (6) (7) (8) (9) (10) (11) (12) $ M_p \text{ (kg)}  0.513  0.516  0.531  0.522  0.525  0.517  0.537  0.516 \\ M_d \text{ (kg)}  0.071  0.076  0.081  0.082  0.085  0.088  0.084  0.079 \\ K_p \text{ (Nm}^{-1)}  477  493  568  584  639  663  619  644 \\ K_d \text{ (Nm}^{-1)}  424  469  491  552  598  601  578  539 \\ A_r \text{ (m}^2)  0.00015  0.000152  0.000156  0.00016  0.000169  0.00017  0.00016  0.00017 \\ \hline Design parameter & & & & & & & & & & & & & & & & & & &$	Di	Real Values of Dominant Poles							
$\begin{array}{c ccccccccccccccccccccccccccccccccccc$	Design parameter	(5)	(6)	(7)	(8)	(9)	(10)	(11)	(12)
$\begin{array}{c ccccccccccccccccccccccccccccccccccc$	$M_p$ (kg)	0.513	0.516	0.531	0.522	0.525	0.517	0.537	0.516
$ \begin{array}{ c c c c c c c c c c c c c c c c c c c$	$M_d$ (kg)	0.071	0.076	0.081	0.082	0.085	0.088	0.084	0.079
$\begin{array}{c ccccccccccccccccccccccccccccccccccc$	$K_p  (\mathrm{Nm}^{-1})$	477	493	568	584	639	663	619	
$\begin{array}{ c c c c c c c c c c c c c c c c c c c$	$K_d  (\mathrm{Nm}^{-1})$	424	469	491	552	598	601	578	539
Design parameter (13) (14) (15) (16) (17) $ M_p \text{ (kg)} \qquad 0.525 \qquad 0.518 \qquad 0.533 \qquad 0.511 \qquad 0.528 \\ M_d \text{ (kg)} \qquad 0.08 \qquad 0.083 \qquad 0.087 \qquad 0.081 \qquad 0.079 \\ K_p \text{(Nm}^{-1}) \qquad 658 \qquad 603 \qquad 630 \qquad 639 \qquad 620 \\ K_d \text{(Nm}^{-1}) \qquad 601 \qquad 589 \qquad 601 \qquad 593 \qquad 600 \\ A_r \text{ (m}^2) \qquad 0.000173  0.00017  0.000172  0.000168  0.000166 $	$A_r (\mathrm{m}^2)$	0.00015	0.000152	0.000156	0.00016	0.000169	0.00017	0.00016	0.00017
$\begin{array}{c ccccccccccccccccccccccccccccccccccc$	Degian namenatan			Real	Values of D	ominant Po	les		
$\begin{array}{c ccccccccccccccccccccccccccccccccccc$	Design parameter	(13)	(14)	(15)	(16)	(17)			
$\begin{array}{c ccccccccccccccccccccccccccccccccccc$	$M_p$ (kg)	0.525	0.518	0.533	0.511	0.528			
$\begin{array}{c ccccccccccccccccccccccccccccccccccc$	$M_d$ (kg)	0.08	0.083	0.087	0.081	0.079			
$K_d  (\mathrm{Nm^{-1}})$ $601$ $589$ $601$ $593$ $600$ $0.000173$ $0.000172$ $0.000168$ $0.000166$	$K_p(\mathrm{Nm}^{-1})$	658	603	630	639	620			
0.53 0.52 0.51 0.52 0.52 0.52 0.6 8 10 12 14 16 Real value 0.47 0.46 8 10 12 14 16 Real value	$K_d  (\mathrm{Nm}^{-1})$	601	589	601	593	600			
0.52 1.1 0.52 0.51 0.50 0.51 0.50 0.50 0.60 0.40 0	$A_r  (\mathrm{m}^2)$	0.000173	0.00017	0.000172	0.000168	0.000166			
6 8 10 12 14 16 6 8 10 12 14 16 Real value	1.1- 05- 1- 95-		, o o o		Power piston velocity (m/s)	51-			
(a)    (b)	6 8 10		14 16		0.4	46 6			14 16
		$(\mathbf{a})$					(b	<b>o</b> )	

Fig. 7. The effect of changing the real amount on the maximum velocity of pistons (a) displacer piston (b) power piston.



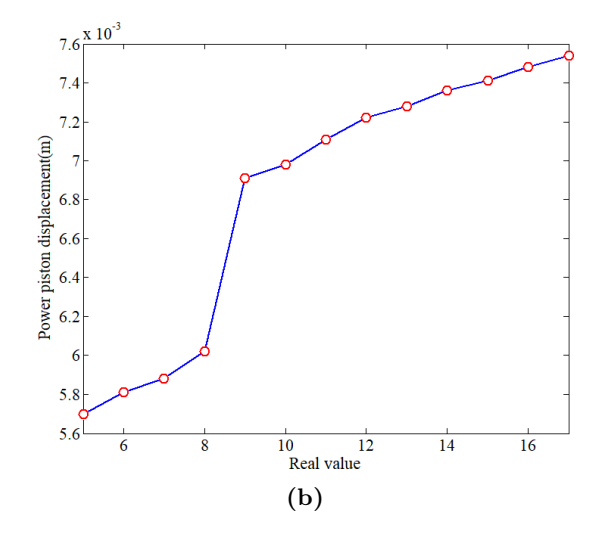
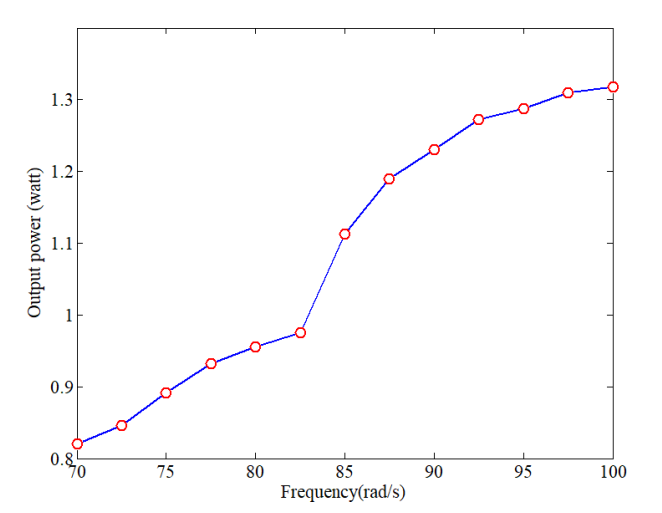


Fig. 8. The effect of changing the real amount on the maximum amplitude of pistons (a) displacer piston (b) power piston.



63.5 63-62-61.5-

Fig. 9. The effect of frequency variation on engine output power.

Fig. 11. The effect of frequency variation on phase difference between pistons.

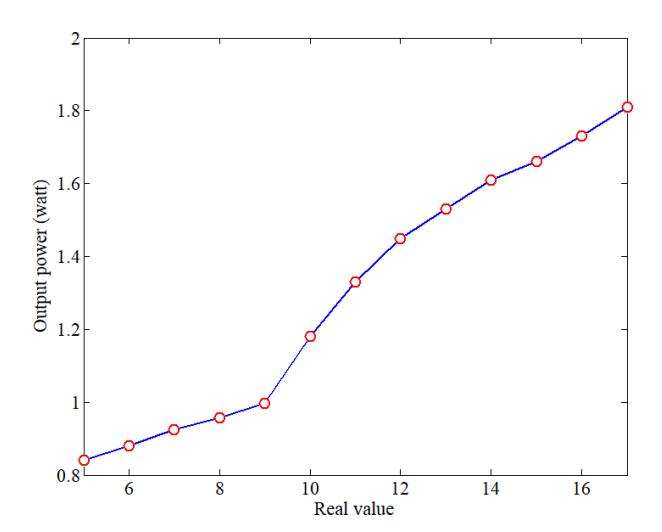


Fig. 10. The effect of real value variation on engine output power.

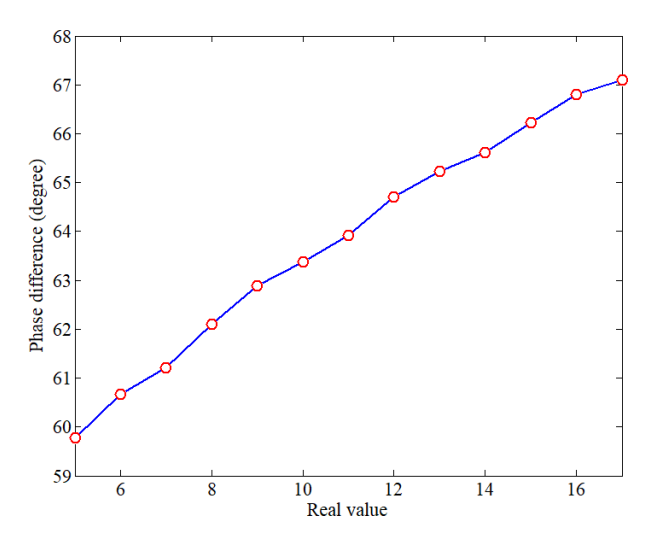


Fig. 12. The effect of real value variation on the phase difference between pistons.

### 5 Conclusion

In this paper, the performance of a FPSO was evaluated and assessed for the first time using a fifth-order model. Initially, an introduction to the free-piston Stirling oscillator was provided. Subsequently, considering the limited heat transfer coefficient, a fifth-order mechanical model was derived, incorporating the system's closed-loop matrix. Five design parameters were considered: the stiffness of the springs, the mass of the displacer and power pistons, and the cross-sectional area of the rod connecting to the displacer piston. The values of these design parameters were then estimated based on two primary objectives: a desired frequency range of 70 to 100 rad/s and a real value of the dominant closed-loop poles between 5 and 17, using the fifth-order mechanical model. Following this, nonlinear analysis was conducted to examine the effects of varying frequency and the real part of the dominant closedloop poles on the output power and the phase difference between the pistons. The results of this study demonstrated that the fifth-order model provides a more accurate evaluation of the dynamic behavior of FPSOs, offering improved insight into their performance. Overall, the main achievements of this research are as follows:

- Designing a FPSO based on the desired frequency using the fifth-order model.
- Designing a FPSO based on the desired real value of the dominant poles using the fifth-order model.
- Investigating the impact of changing the frequency on output power and phase difference between the pistons using the fifth-order model and nonlinear dynamics.
- Examining the effect of varying the real part of

the dominant poles on output power and phase difference between the pistons using the fifthorder model and nonlinear dynamics.

#### Nomenclature

- A Cross cross-sectional area of the piston and displacer  $(m^2)$
- $A_r$  Cross sectional-area of the displacer rod (m<sup>2</sup>)
- $A_c$  Area of heat sink (m<sup>2</sup>)
- $A_h$  Area of heat source (m<sup>2</sup>)
- $A_{\text{wall}}$  Area on the chamber between the hot and cold (m<sup>2</sup>)
  - b Damping coefficient between displacer rod and power piston potion  $(Nsm^{-1})$
- $b_d$  The damping coefficient of the displacer (Nsm<sup>-1</sup>)
- $b_p$  The damping coefficient of the power piston (Nsm<sup>-1</sup>)
- H Enthalpy (J)
- $h_c$  Heat transfer coefficient of the cold source (WK<sup>-1</sup>m<sup>-2</sup>)
- $h_h$  Heat transfer coefficient of heat source  $(WK^{-1}m^{-2})$
- $h_{\text{wall}}$  Heat transfer coefficient of the chamber between the hot and cold (WK<sup>-1</sup>m<sup>-2</sup>)
- $K_d$  Spring stiffness of displacer (Nm<sup>-1</sup>)
- $K_p$  Spring stiffness of power piston (Nm<sup>-1</sup>)
- M Gas mass (kg)
- $M_d$  Displacer mass (kg)
- $M_p$  Power piston mass (kg)
- P Linear pressure (Pa)
- $P_0$  Initial pressure of working gas (Pa)
- $\hat{P}$  Nonlinear pressure (Pa)
- R Ideal gas constant (Jkg<sup>-1</sup>K<sup>-1</sup>)
- T Temperature (K)
- $T_h$  Hot gas temperature (K)
- $T_c$  Cold gas temperature (K)
- W Work (J)
- $V_h$  expansion space (m<sup>3</sup>)
- $V_{h0}$  The initial volume of expansion space (m<sup>3</sup>)
- $V_c$  compression space (m<sup>3</sup>)
- $V_{c0}$  The initial volume of compression space (m<sup>3</sup>)
- $V_r$  regenerator volume (m<sup>3</sup>)
- x Displacer piston displacement (m)
- $\dot{x}$  Displacer velocity (ms<sup>-1</sup>)
- y Power piston displacement (m)
- $\dot{y}$  Power piston velocity (ms<sup>-1</sup>)

#### Greek symbols

- $\gamma$  Heat capacity ratio
- $\omega$  Frequency (rad/s)

## Acknowledgment

The authors would like to express their sincere gratitude to the Iranian Research Organization for Science and Technology (IROST) for providing the necessary facilities and support. This research was supported by IROST under Grants No. 034551, 034566, 034549 and 034542.

#### References

- Zare S, Pourfayaz F, Tavakolpour-Saleh A, Lashaki RA. A design method based on neural network to predict thermoacoustic Stirling engine parameters: Experimental and theoretical assessment. Energy. 2024;309:133113.
- [2] Moradi N, Boroujeni NM. Prize-collecting Electric Vehicle routing model for parcel delivery problem. Expert Systems with Applications. 2025:259:125183.
- [3] Walker G, Senft JR, Walker G, Senft J. Freepiston Stirling engines. Springer; 1985.
- [4] Shourangiz-Haghighi A, Diazd M, Zhang Y, Li J, Yuan Y, Faraji R, et al. Developing more efficient wind turbines: A survey of control challenges and opportunities. IEEE Industrial Electronics Magazine. 2020;14(4):53-64.
- [5] Zare S, Tavakolpour-Saleh A, Binazadeh T. Analytical investigation of free piston Stirling engines using practical stability method. Chaos, Solitons & Fractals. 2023;167:113082.
- [6] Dashti E, Tabari NG, Zare S, Shabanpour H. An analytical investigation of a thermoacoustic stirling engine. Arabian Journal for Science and Engineering. 2024;49(8):11073–11090.
- [7] Ulusoy N. Dynamic analysis of free piston Stirling engines. Case western reserve university; 1994.
- [8] Zare S, Tavakolpour-Saleh A, Hosseininia A, Sangdani MH. Investigating the onset and steady-state conditions of a diaphragm thermoacoustic stirling engine. Proceedings of the Institution of Mechanical Engineers, Part A: Journal of Power and Energy. 2024;238(4):731–760.

- [9] Dai Z, Wang C, Zhang D, Tian W, Qiu S, Su G. Design and analysis of a free-piston stirling engine for space nuclear power reactor. Nuclear Engineering and Technology. 2021;53(2):637–646.
- [10] Jiang Z, Yu G, Zhu S, Dai W, Luo E. Advances on a free-piston Stirling engine-based micro-combined heat and power system. Applied Thermal Engineering. 2022;217:119187.
- [11] Zare S, Tavakolpour-Saleh A. Free piston Stirling engines: A review. International Journal of Energy Research. 2020;44(7):5039–5070.
- [12] Zare S, Tavakolpour-Saleh A, Aghahosseini A, Mirshekari R. Thermoacoustic Stirling engines: A review. International Journal of Green Energy. 2023;20(1):89-111.
- [13] Riofrio JA, Al-Dakkan K, Hofacker ME, Barth EJ. Control-based design of free-piston stirling engines. In: 2008 American Control Conference. IEEE: 2008. p. 1533–1538.
- [14] Hofacker ME, Tucker JM, Barth EJ. Modeling and validation of free-piston Stirling engines using impedance controlled hardware-in-the-loop. In: Dynamic systems and control conference. vol. 54754; 2011. p. 153–160.
- [15] Zare S, Tavakolpour-Saleh A. Frequency-based design of a free piston Stirling engine using genetic algorithm. Energy. 2016;109:466–480.
- [16] Der Minassians A, Sanders SR. Multiphase stirling engines; 2009.
- [17] Zare S, Tavakolpour-Saleh A. Applying particle swarm optimization to study the effect of dominant poles places on performance of a free piston Stirling engine. Arabian Journal for Science and Engineering. 2019;44:5657–5669.
- [18] Bégot S, Layes G, Lanzetta F, Nika P. Stability analysis of free piston Stirling engines. The European Physical Journal-Applied Physics. 2013;61(3):30901.

- [19] Shourangiz-Haghighi A, Tavakolpour-Saleh A. A neural network-based scheme for predicting critical unmeasurable parameters of a free piston Stirling oscillator. Energy Conversion and Management. 2019:196:623–639.
- [20] Azghan RR, Glodosky NC, Sah RK, Cuttler C, McLaughlin R, Cleveland MJ, et al. Personalized modeling and detection of moments of cannabis use in free-living environments. In: 2023 IEEE 19th International Conference on Body Sensor Networks (BSN). IEEE; 2023. p. 1–4.
- [21] Alsadat SM, Baharisangari N, Paliwal Y, Xu Z. Distributed reinforcement learning for swarm systems with reward machines. In: 2024 American Control Conference (ACC). IEEE; 2024. p. 33–38.
- [22] Glodosky NC, Cleveland MJ, Azghan RR, Ghasemzadeh H, McLaughlin RJ, Cuttler C. Multimodal examination of daily stress rhythms in chronic Cannabis users. Psychopharmacology. 2024;p. 1–24.
- [23] Alsadat SM, Gaglione JR, Neider D, Topcu U, Xu Z. Using large language models to automate and expedite reinforcement learning with reward machine. arXiv preprint arXiv:240207069. 2024;.
- [24] Azghan RR, Glodosky NC, Sah RK, Cuttler C, McLaughlin R, Cleveland MJ, et al. CUDLE:

- Learning Under Label Scarcity to Detect Cannabis Use in Uncontrolled Environments. arXiv preprint arXiv:241003211. 2024;.
- [25] Perozziello C, Grosu L, Vaglieco BM. Free-piston stirling engine technologies and models: A review. Energies. 2021;14(21):7009.
- [26] Qiu S, Gao Y, Rinker G, Yanaga K. Development of an advanced free-piston Stirling engine for micro combined heating and power application. Applied energy. 2019;235:987–1000.
- [27] Zare S, Tavakol Poursaleh AR. Nonlinear dynamic analysis of solar free piston hot-air engine. Modares Mechanical Engineering. 2015;15(9):223– 234.
- [28] Ye W, Wang X, Liu Y. Application of artificial neural network for predicting the dynamic performance of a free piston Stirling engine. Energy. 2020;194:116912.
- [29] Zare S, Tavakolpour-Saleh A, Binazadeh T. Passivity based-control technique incorporating genetic algorithm for design of a free piston Stirling engine. Renewable Energy Focus. 2019;28:66–77.
- [30] Martinez Saturno JG. Some mathematical models to describe the dynamic behavior of the B-10 free-piston stirling engine; 1994.